ELSEVIER

Journal of Nuclear Materials 266–269 (1999) 1139–1144

journal of nuclear materials

Influence of magnetic configuration and heating methods on distribution of diverted plasmas in Heliotron E

T. Mizuuchi [a,*], V.S. Voitsenya [b], V.V. Chechkin [b], K. Nagasaki [a], H. Zushi [c], M. Nakasuga [d], H. Okada [a], S. Besshou [d], A. Hayakawa [a], H. Funaba [e], T. Hamada [a], S. Masuzaki [e], K. Kondo [d], F. Sano [a], O. Motojima [e], O.S. Pavlichenko [b], T. Obiki [a]

[a] *Institute of Advanced Energy, Kyoto University, Gokasho, Uji 611-0011, Japan*
[b] *Institute of Plasma Physics, NSC Khar'kov Institute of Physics and Technology, 310108 Khar'kov, Ukraine*
[c] *Research Institute for Applied Mechanics, Kyushu University, Kasuga 816-0811, Japan*
[d] *Graduate School of Energy Science, Kyoto University, Gokasho, Uji 611-0011, Japan*
[e] *National Institute for Fusion Science, 322-6 Oroshi-cho, Toki-shi 509-5202, Japan*

Abstract

A study on the distribution of the amount of diverted plasma along torus in Heliotron E was performed for NBI and ECH plasmas under different experimental conditions. A strong up–down asymmetry of the diverted plasma flux was observed contrary to what should be expected from the vacuum magnetic configuration. The degree of this asymmetry depends on the discharge conditions. This result indicates that the knowledge of only vacuum field traces in a divertor region is not enough to predict how much ratio of the total diverted plasma comes to a concerning divertor section in the heliotron/torsatron devices.

Keywords: Heliotron E; Divertor; Helical divertor; Plasma edge

1. Introduction

A critical issue of the divertor concept is to control heat and particle flux to the divertor plate. The knowledge of the spatial and quantitative distribution of the divertor heat- and particle-flux is necessary to develop the divertor control method. In heliotron/torsatron devices, the edge magnetic structure can be used as the divertor field without any additional coil systems ('natural' divertor). Since the confinement field is created only by the external coils, numerical traces of the vacuum field lines can predict the 'location' of the divertor flux bundles. In contrast to the scrape-off layer (SOL) in 'ideal' (non-perturbed) tokamaks, many islands are coupled to each other in the divertor field of a heliotron/torsatron device resulting in a 'stochastic' non-axisymmetric region. For such a device, can we predict a detailed quantitative distribution of divertor plasma along the divertor trace only from a vacuum field calculation? The existence of a microstructure in the scrape-off 'region' would modify the divertor particle-flux distribution through the change of edge plasma profile. A local heating source/sink can affect the distribution as demonstrated in experiments in Uragan-3M [1]. Even in tokamaks, the same situation can happen in principle since some error fields or MHD activities can transform the laminar SOL to a stochastic scrape-off region [2,3]

The previous experiments in Heliotron E shows that the observed diverted plasma position agree with the region where the vacuum field line has longer wall-to-wall connection length, Lc ($Lc >$ a few meters) [4,5]. However, there is little discussion on how much ratio of the total diverted plasma comes to each divertor target along the torus. In this paper, we discuss the difference of the amount of the diverted plasma along the divertor trace based on recently performed measurements for

* Corresponding author. Tel: +81 774 38 3451; fax: +81 774 38 3535; e-mail: t-mizuuchi@iae.kyoto-u.ac.jp

0022-3115/99/$ – see front matter
PII: S0022-3115(98)00686-2

ECH and NBI plasmas under different experimental conditions in Heliotron E.

2. Experimental setup

Heliotron E is an $\ell = 2/m = 19$ helical heliotron device [6]. The plasma major and minor radii for the standard configuration are $R_0 = 2.21$ m and $\langle a \rangle \approx 0.2$ m, respectively. The last closed flux surface (LCFS) is restricted by the magnetic limiter and the positions of the 'X-point-like' structure of the edge magnetic field are well inside of the vacuum chamber. In this experiment, currentless plasmas were produced by the fundamental (53.2 GHz, $\lesssim$0.4 MW) or the 2nd harmonic (106.4 GHz, $\lesssim$0.3 MW) ECH [7] mainly under the inward shifted configuration of $R_0 = 2.18$ m with the magnetic field of $|B_0| = 1.9$ T. The plasma was supported and heated by NBI (total injected power, $P_{\rm inj}$, $\lesssim 3$ MW, a pulse length $\lesssim$ 160 ms). The second pulse of ECH ($\lesssim$40 ms) was superimposed on NBI plasmas in some cases. The location of the heating sources along the torus is shown schematically in Fig. 1. The typical values of the central chord-averaged electron density, the electron and ion temperatures were $\bar{n}_{\rm e} \approx (1.0 - 2.5) \times 10^{19} {\rm m}^{-3}$, $T_{\rm e}(0) \approx 0.6 - 1.5$ keV and $T_{\rm i}(0) \approx 0.3 - 0.6$ keV, respectively.

As a measure of the amount of diverted plasma, the ion saturation current (not current density), $I_{\rm S}$, to the plane collectors in eight arrays located near the wall at four poloidal cross-sections was used [4,8,9]. Every array consists of seven collectors and it is identified by the poloidal angle Θ of its center: $\Theta = 0°$, 45°, 90°, 135°, 180°, 225°, 270°, and 315° (see Fig. 1). All collectors in the arrays were biased to -120 V against the potential of the vacuum chamber. Calculated footprints of the vacuum divert or field lines on the chamber wall are shown in Fig. 2 for a standard configuration and the position of the eight collector arrays is also indicated (shaded rectangles in the figure).

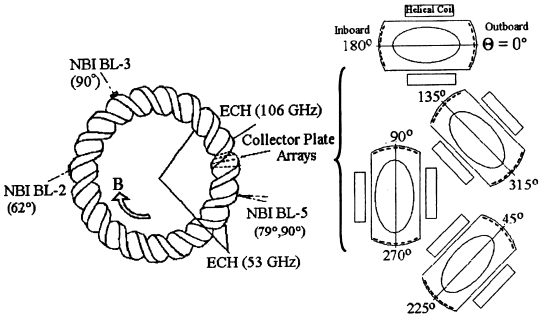

Fig. 1. Location of heating sources (NBI, ECH) and collector–plate arrays (Left). The details of the collector–plate arrays (Right).

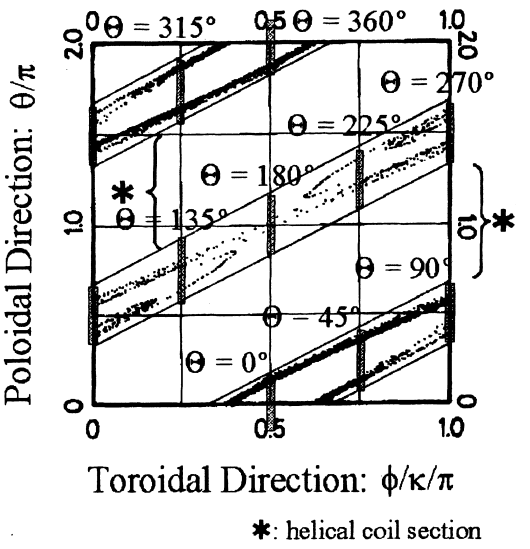

Fig. 2. Calculated footprints of the field lines on the wall surface (dots). θ and ϕ are the poloidal and toroidal angles, respectively. κ is the poloidal rotation number of the helical coil ($\theta = \kappa\phi$). The shaded rectangles denote the positions of the collector–plate arrays.

3. Global characteristics of the diverted plasma distribution along the torus

The diverted plasma comes to the collectors from two directions: parallel and anti-parallel to the field line. These two flows are clearly separated and detected by different collectors in outboard, top, and bottom arrays ($\Theta = 0°$, 45°, 90°, 270°, and 315°) but it is difficult to separate them in $\Theta = 135°$, 180°, and 225° arrays. To avoid this inconvenience and to discuss the uniformity of the amount of the diverted plasma distributed along the helical path of the divertor trace, the 'total value of the density-normalized divertor particle-flux' for each array is defined by the summation of I_S of each array, $\Gamma(\Theta, t) \equiv \Sigma[I_S(\theta, t)/\bar{n}_{\rm e}(t)]$. Here, the normalization of $I_S(\theta, t)$ by $\bar{n}_{\rm e}$ is performed to reduce the error due to the reproducibility of plasmas since more than eight similar shots were necessary to obtain a full set of $\Gamma(\Theta)$ due to the limited channel number of data acquisition. The poloidal distance between the adjacent collector plates in each array are rather small (2–4 mm). Therefore, $\Gamma(\Theta) \times \langle \bar{n}_{\rm e} \rangle$ can be used as a measure of total diverted particles coming to the array at Θ even if the poloidal width of the diverted plasma flow is increased by the enhanced diffusion or the strike points shift by the change of the field configuration. Here, $\langle \bar{n}_{\rm e} \rangle$ is the mean value of for shots required to obtain a full set of $\Gamma(\Theta)$.

Fig. 3 shows a typical distribution of $\Gamma(\Theta)/\Gamma(\Theta = 270°)$ for the NBI plasma in a configuration of $R_0 = 2.18$ m. As shown in Fig. 3, the value of $\Gamma(\Theta)$ is not constant along the divertor trace (along Θ). Some of the observed

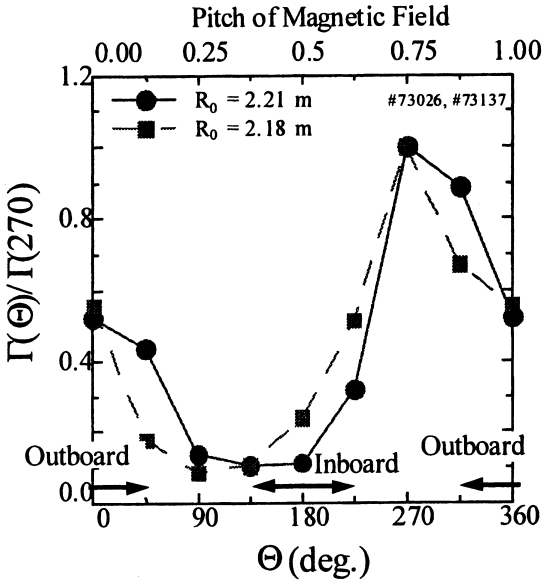

Fig. 3. Typical $\Gamma(\Theta)$ profile for two different values of the additional vertical field conditions. $R_0 = 2.21$ and 2.18 m.

non-uniformity arises from the characteristic of the field configuration. As shown in Fig. 2, the 'density' of the footprints of the divertor field lines is not uniform along the torus. Therefore, it is natural to consider that $\Gamma(\Theta)$ also changes along the torus. The important feature of Fig. 3 is the asymmetry of $\Gamma(\Theta)$, which is observed between diverted plasmas at geometrically symmetric positions; $\Theta = 45°/315°$, 90°/270°, and 135°/225°. To characterize the asymmetry of the $\Gamma(\Theta)$ distribution, the ratios of $\Gamma_{up}/\Gamma_{down}$ and Γ_{in}/Γ_{out} are evaluated, where:

$$\Gamma_{up} = \Gamma(45°) + \Gamma(90°) + \Gamma(135°),$$
$$\Gamma_{down} = \Gamma(225°) + \Gamma(270°) + \Gamma(315°),$$
$$\Gamma = \Gamma(180°) + \Gamma(135°) + \Gamma(225°) \text{ and}$$
$$\Gamma_{out} = \Gamma(45°) + \Gamma(315°) + \Gamma(0°).$$

4. Effects of the magnetic configuration

The magnetic configuration can be controlled by using auxiliary fields in Heliotron E [6]. The additional vertical field, B_{AV}, mainly leads to the horizontal shift of the magnetic axis. The additional toroidal field, B_{AT}, mainly changes the size of LCFS, the rotational transform and the magnetic shear. The distribution of $\Gamma(\Theta)$ was affected by these additional fields.

In Fig. 3, $\Gamma(\Theta)/\Gamma(270°)$ for the configuration of $R_0 = 2.21$ m is also plotted. Comparing distributions for two configurations, it is seen that $\Gamma(\Theta)/\Gamma(270°)$ for the outboard arrays ($\Theta = (0°)$, 45° and 315°) are decreased and that for the inboard arrays ($\Theta = 135°$, 180° and 225°) are increased by the inward shift of the magnetic axis. The difference between Γ_{in} and Γ_{out} decreased with an increase of the inward shift. In order to explain these observations, we should check the deformation of the edge structure by the additional vertical field, besides the discussion on the local modification of the core plasma transport. Fig. 4 shows Lc of the vacuum fields starting from each array for the two configurations. The width of long Lc region for the inboard arrays is increased and

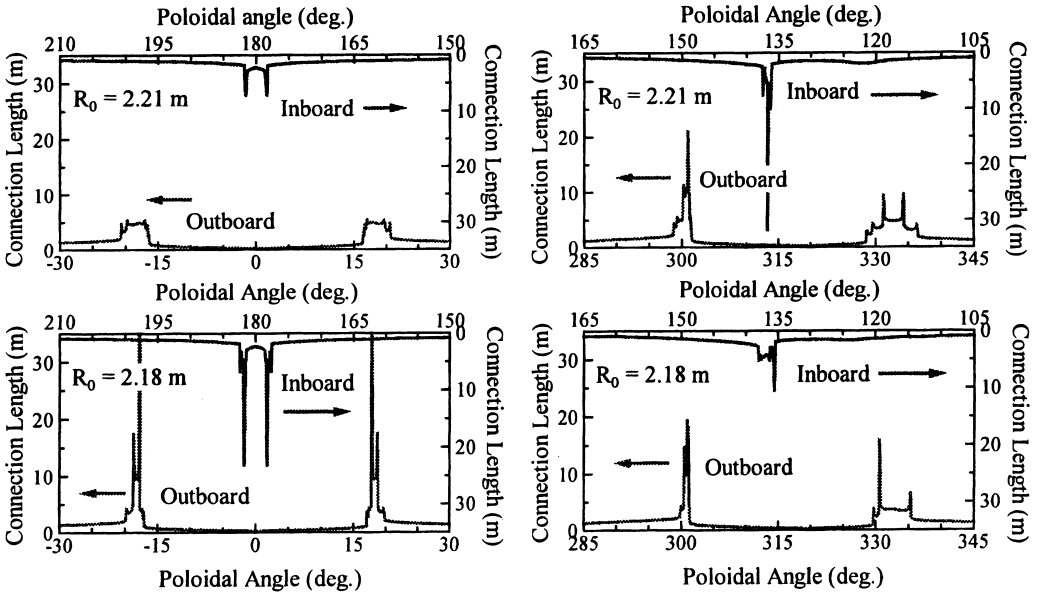

Fig. 4. Effect of the horizontal shift on the connection length of the field line at $\Theta = 0°$,135°,180°,315° arrays.

that for the outboard arrays is decreased by the inward shift. However, the change of Lc itself is not related to the observed change of the diverted plasma distribution.

As for the up–down asymmetry, the ratio of $\Gamma(90°)/\Gamma(270°)$ became unity when the size of LCFS was reduced to ~85% by B_{AT}. This ratio is also affected by B_{AV} (or the value of R_0). The highest up–down asymmetry under the $B_{AT}=0$ condition was observed at the $R_0=2.18$ m configuration. The vacuum field calculation shows B_{AV} has also a slight effect on the size of LCFS and the rotational transform. The $R_0=2.18$ m configuration has the maximum $\langle a\rangle$ under the $B_{AT}=0$ condition (~6% increase from the standard configuration). These observations suggest the size of LCFS and/or the edge rotational transform may affect the toroidal distribution of the divertor flow.

5. Effect of the plasma heating on the divertor flow distribution

Fig. 5 shows an example of the time traces of $\Gamma_{total}(t)=\Sigma\Gamma(\Theta,t)$, Γ_{in}/Γ_{out}, and $\Gamma_{up}/\Gamma_{down}$ with the central chord-integrated electron line-density, $n_e\ell$, and the time history of the plasma heating. Since $\Gamma(\Theta)$ is normalized by the core density, $\Gamma_{total}=\Sigma\Gamma(\Theta)$ can be considered as a measure of the total plasma loss rate from the core region. In the discharge of Fig. 5, the plasma was produced by 53 GHz ECH (~0.3 MW) and heated by NBI ($P_{inj}\sim 1.2$ MW). In the last 30 min, NBI power increased up to $P_{inj}\sim 2.3$ MW. During the first stage of NBI, the second pulse of 53 GHz ECH (~0.4 MW) was imposed. As shown in Fig. 5, the plasma loss, Γ_{total}, increases when P_{inj} increases or ECH is overlapped. These responses to the heating power might be related to so-called power degradation of the plasma confinement [10,11].

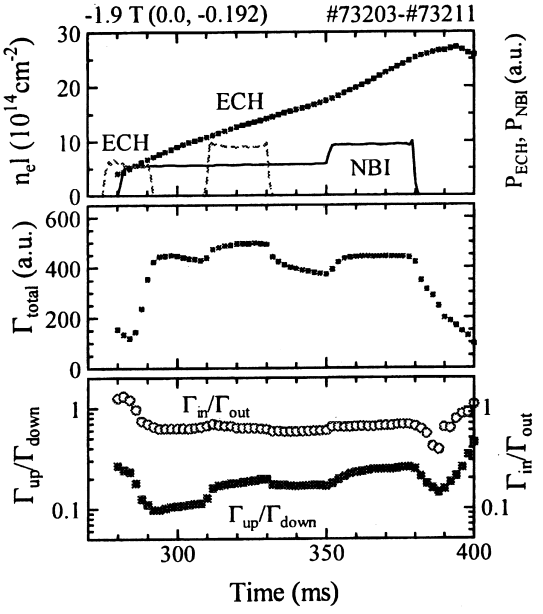

Fig. 5. Time traces of $n_e\ell$, Γ_{total}, Γ_{in}/Γ_{out} and $\Gamma_{up}/\Gamma_{down}$. In the top column, the timing of ECH and NBI is also plotted.

As for the Θ-profile of $\Gamma(\Theta)$, the ECH pulse during NBI increases the ratios of $\Gamma_{up}/\Gamma_{down}$ and Γ_{in}/Γ_{out}. The raise of NBI power also increases these ratios. It is interesting to note the change of $\Gamma_{up}/\Gamma_{down}$ and Γ_{in}/Γ_{out} in the after-glow plasma. These ratios decrease just after the turn-off of the heating power and gradually increase after ~10 ms from the power-off. In order to explain this behavior in the after-glow phase, it would be necessary to consider the effects of rapid temperature drop, reduction of high-energy injected particles and increase of neutrals.

To check the effect of the plasma heating on the $\Gamma(\Theta)$-distribution, the power dependence of $\Gamma(\Theta)$ was investigated. In Fig. 6, $\Gamma(\Theta)$ is plotted as a function of the absorbed power normalized to the mean plasma density, $P_{abs}/\bar{n}_e$. The data for three different phases of the discharge are plotted: • – at the early NBI phase (320 ms $\lesssim t\lesssim$ 340 ms, NBI-1), ▼ – during NBI + ECH phase (NBI-1 + ECH), and □ – at the later NBI phase (370 ms $\lesssim t\lesssim$ 440 *ms*, NBI-2). In spite of a wide spread of data, for the NBI-1 phase, $\Gamma(\Theta)$ seems to be scaled by a linear function of $P_{abs}/\bar{n}_e$. For the NBI-2 phase, $\Gamma(\Theta)$ seems to be in the range of this scaling.

As shown in Fig. 6, the second pulse of ECH on NBI increases $\Gamma(\Theta)$. The increment by the ECH is, however, not the same for each array and for the ECH frequencies [12]. For 106 GHz ECH, $\Gamma(\Theta)$ was close to the scaled value by the relation for NBI-1. For 53 GHz ECH,

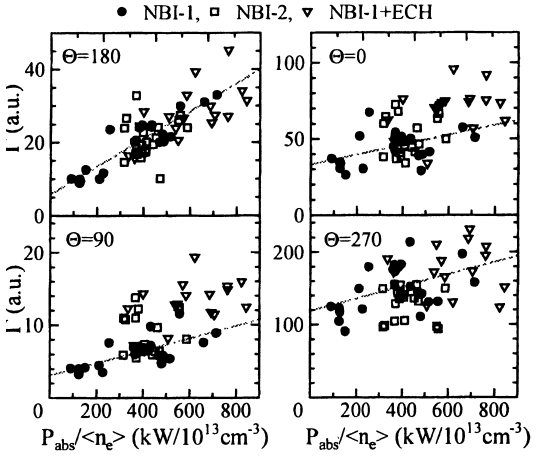

Fig. 6. $P_{abs}/\bar{n}_e$ dependence of $\Gamma(\Theta)$ at $\Theta=0°$, 90°, 180°, 270° for different phases of a discharge; NBI-1 (•), NBI-1+ ECH (▼), and NBI-2 (□).

however, a significant increase of $\Gamma(\Theta)$ was observed at some Θ positions. The differences between these two ECHs are (1) a fundamental resonance for 53 GHz ECH and the second harmonic resonance for 106 GHz ECH, (2) a significant amount of the microwave power deposited at the peripheral region for 53 GHz ECH due to its beam pattern. For the NBI and the 106 GHz ECH cases, the major of the power is absorbed in the central region.

6. Discussion

One of the special features of the distribution of diverted plasma near the wall in Heliotron E is the up–down asymmetry which cannot be explained by the 'ideal' field configuration. This asymmetry depends not only on the field configuration but also on the conditions of plasma production and heating. The relaxation or reversal of the asymmetry has been observed in two cases. In the first case, the size of LCFS was decreased by B_{AT}. In the second case, the direction of confinement field was reversed.

One possible reason of the up–down asymmetry is a scraping of divertor flows by some obstacles in the vacuum chamber. One candidate of such obstacles is a limiter located on the bottom of the torus at one helical pitch apart from the $\Theta = 270°$ section. (The limiter was extracted in this study and the distance between LCFS and the leading limiter edge was ~4 cm.) However, the field calculation for the 'ideal' vacuum condition shows that the limiter makes almost no shadows on collector plates.

Another possibility is the deformation of the edge structure by some perturbation field [12]. In double-null divertor tokamaks, a small perturbation field can break a separatrix into two (inner and outer) separatrixes and cause a large up–down asymmetry of the divertor flow distribution [13]. Even in heliotron/torsatron devices, similar deformation might be possible. Moreover, if such a deformation (the up–down asymmetry of the field configuration) exists, the asymmetric motion of energetic particles produced by ECH or NBI can affect the diverted plasma and its distribution [14]. In Heliotron E, there is no experimental evidence of up (or down) shift of the plasma column. However, the possibility of the distortion of the edge magnetic surface around the rational surface of $\iota/2\pi = 2.5$ and/or 2.0 is discussed in [15]. The low mode islands near LCFS would work as the 'breaking' of the separatrix.

From the fact that the $\Gamma(\Theta)$-distribution depends on the heating conditions, one might consider the effects of plasma β and/or plasma current as an explanation. In principle, the plasma shift by a finite β-effect and/or the change of the rotational transform or the shear by the plasma current can modify the edge structure and then change the $\Gamma(\Theta)$ distribution. In Heliotron E, the shift of LCFS caused by β-effect is less than a few mm and the plasma current is the order of 10 kA or less [16]. Owing to the peculiarity of the Heliotron E geometry, these values seem to be too small to create a significant change in the outline of the long Lc region. However, these might make a change of the microstructure in the long Lc region and cause re-distribution of the diverted plasma along the divertor trace.

The changes of $\Gamma(\Theta)$-distribution observed during different discharge-stages may be explained also from the viewpoint of the plasma transport or the characteristic of plasma heating. A local change of the plasma potential induced by NBI or ECH can make asymmetric plasma loss. The biased limiter experiment in Heliotron E showed that the divertor flow was affected by an artificial modification of the edge plasma potential [17]. As discussed in [1], a local heating source can affects the local plasma potential and shift the diverted plasma flow from the original position. The effects of the local heating on the potential distribution at the divertor region and on the SOL current in Heliotron E are under investigation.

As for the plasma transport, not only an asymmetric increase of transport but also a symmetric increase may change the diverted plasma distribution in the case where the SOL has some 'microstructure'. In such a case, the change of the edge plasma profile should cause re-distribution of the divertor flow. For the NBI + ECH phase, the increase of SOL radial decay length was observed [18]. This expansion of the edge plasma by ECH overlapping might relate to the change of divertor flow distribution.

7. Summary

A comprehensive study on the distribution of divertor particle-flux flows in Heliotron E was performed under different experimental conditions. The following are observed

1. The amount of the diverted plasma along the divertor trace was not uniform for all experimental conditions.
2. The asymmetric distribution of the diverted plasma at the geometrically symmetric positions was found.
3. The degree of the asymmetry depends not only on the vacuum magnetic configuration but also on other discharge conditions; methods and power of plasma heating.

Some possible reasons for the up–down asymmetry of the diverted plasma are discussed. However, a clear-cut picture for the mechanisms of the observed asymmetry is still not obtained. More detailed analyses and simulations are necessary. We must keep in mind that knowledge of the vacuum field mapping in a divertor

region is not enough to predict how much ratio of the diverted plasma comes to a concerning divertor target.

Acknowledgements

This work was performed in collaboration with IAE, IPP-NSC-KIPT and NIFS. The authors acknowledge everyone who supported this collaboration. They are grateful to Heliotron E operation staff for their excellent support. Helpful discussions with Dr M. Smirnova from IFP and Dr E.L. Sorokovoj are also acknowledged.

This work was partially supported by the Collaboration Program of the Laboratory for Complex Energy Processes, IAE, Kyoto University.

References

[1] V.Ye. Bykov, V.V. Chechkin, et al., Plasma Phys. Control. Fusion 37 (1995) 271.
[2] T.E. Evans, C.J. Lasnier, D.N. Hill, et al., J. Nucl. Mater. 220–222 (1995) 235.
[3] T.E. Evans and the ASDEX Team, IPP III/154 (March 1991).
[4] T. Mizuuchi, H. Matsuura, K. Konda et al., Proc. 18th EPS Conf. Contr. Fusion Plasma Phys. (Berlin, 1991). Vol. 5C, part III (EPS, Geneva, 1991) p. 65; Proc. 8th Int. Conf. Stellarators (Kharkov, 1991), (IAEA, Vienna, 1991) 365.
[5] T. Obiki, T. Mizuuchi, H. Zushi et al., Plasma Phys. Control. Fusion Research 1998, vol. 2 (IAEA, Vienna, 1989) p. 337.
[6] T. Obiki, M. Wakatani, M. Wakatani, M. Sato, et al., Fusion Tech. 17 (1990) 101.
[7] T. Mizuuchi, H. Zushi, K. Nagasaki, et al., Proc. ICPP96, Nagoya, 1996, vol. 1, p. 1018.
[8] V.V. Chechkin, et al., Proc. 24th EPS Conf. Contr. Fusion Plasma Phys. (Berchestgarden, 1997) vol. 21A, part IV (EPS, Geneva, 1991) p. 1841.
[9] V.S. Voitsenya, et al., ibid part II (EPS, Geneva, 1991) p. 901.
[10] S. Sudo, et al., Nucl. Fusion 30 (1990) 11.
[11] K. Uchino, T. Koga, K. Muraoka, et al., J. Phys. Soc. Japan, 57 (1988) 909.
[12] V.V. Chechkin, V.S. Voitsenya, et al., Research Report of IAE Kyoto Univ., IAE-RR-98 056, 1998.
[13] R. Marchand, M. Dumberry, Y. Demers, et al., Nucl. Fusion 35 (1995) 297.
[14] P.N. Yushimanov, J.R. Cary, S.G. Shasharina, Nucl. Fusion 33 (1993) 1293.
[15] T. Mizuuchi, H. Matsuura, A. Komori, et al. J. Nucl. Mater. 176&177 (1990) 1070.
[16] S. Besshou, K. Ogata, K. Kondo, et al., Nucl. Fusion 35 (1995) 173.
[17] T. Mizuuchi, K. Kondo., H. Zushi, et al., Proc. 9th Int. Conf. Stellarator (Garching, 1993), (IAEA, Vienna, 1993) 397.
[18] T. Mizuuchi, B.J. Peterson, T. Nakayama, et al., EUR-CIEMAT 30 (1995) 81; Proc. 10th Int. Conf. Stellarators, Madrid, 1995.